Neutron Star Astrophysics at the Crossroads: Magnetars and the Multimessenger Revolution
Proceedings IAU Symposium No. 363, 2023
E. Troja & M. G. Baring, eds.
doi:10.1017/S1743921322000576

The Off-Axis Afterglow of GW170817: Flux Prediction at Very High Energies

Clément Pellouin and Frédéric Daigne

Sorbonne Université, CNRS, UMR 7095, Institut d'Astrophysique de Paris (IAP),
98 bis boulevard Arago, 75014 Paris, France
email: pellouin@iap.fr

Abstract. The binary neutron star merger gravitational-wave event GW170817 and observations of the subsequent electromagnetic signals at different wavelengths have helped better understand the outflows that follow these mergers. In particular, the off-axis afterglow of the jetted ejecta has allowed to probe the lateral structure of such jets, especially thanks to VLBI imagery of the source. In this work, we model this afterglow including a decelerating jet with lateral structure, while synchrotron emission and synchrotron self-Compton scatterings power the jet radiation. In particular, we extend our analysis to very high energies and predict the light curve in the energy range of H.E.S.S. and the CTA. We finally discuss how future detections of afterglows by these observatories can help break the degeneracies in some key physical parameter measurements, and allow to probe efficiently a sub-population of fast-merging binaries.

Keywords. radiation mechanisms: nonthermal, scattering, stars: neutron, gamma rays: bursts

1. Introduction

The first detection of a Binary Neutron Star (BNS) merger by gravitational-wave (GW) interferometers, GW170817 (Abbott et al. 2017a), was followed by several electromagnetic counterparts (Abbott et al. 2017b and references therein). A short Gamma-Ray Burst (GRB) was detected ~ 1.7 s after the GW signal (*e.g.* Goldstein et al. 2017; Sachenko et al. 2017); a fast-decaying thermal transient in the visible/infrared range, the kilonova, was observed for ~ 10 days after the merger (*e.g.* Villar et al. 2017; Tanvir et al. 2017); and a non-thermal afterglow was observed from radio to X-rays for more than three years (see *e.g.* Troja et al. 2020; Hajela et al. 2019).

Compared to the already-known population of cosmological GRBs, GW170817 was much closer (~ 40 Mpc) and seen off-axis. The slow rise of the afterglow light curve until its peak after ~ 100 days hints towards a decelerating jet with a lateral structure, viewed off-axis; though a spherical shell with a radial structure can also fit this behaviour (*e.g.* Gill and Granot 2018). Confirmation of the nature of the afterglow source came with VLBI imagery: its apparent superluminal motion and its compactness brought firm evidence that the source is indeed an ultra-relativistic jet viewed off-axis (Mooley et al. 2018; Ghirlanda et al. 2019). Following these studies, accounting for the lateral structure of the jet in afterglow models has become necessary.

Most models of GW170817's off-axis afterglow emission only assume synchrotron emission at the forward shock and are therefore limited to the spectral range of observations, from radio to X-rays. Discussions on the expected emission in the TeV range are of prime interest in the coming era of the Cerenkov Telescope Array (CTA, see CTA Consortium 2019), that will be sensitive enough to observe some of these afterglows at very high energies. Already, GW170817's afterglow was followed by H.E.S.S. around its peaking

time (at $t \sim 100$ days, see HESS collaboration 2020), and these observations put upper limits on the flux level in the TeV range. In this study, we model GW170817's very high energy afterglow, due to Synchrotron Self-Compton (SSC) emission.

2. Method

Our model to compute the observed afterglow flux uses several components, free parameters and physical assumptions that we briefly describe hereafter:

• **Jet geometry and dynamics.** As indicated by VLBI imaging and the slow rise of the afterglow light-curve, the jetted ejecta is observed off-axis and is laterally structured. We model the structure as a core jet with a given opening angle θ_c and a succession of conic rings surrounding core material, with injection Lorentz factors $\Gamma_0(\theta)$ and injected kinetic energy per solid angle $\epsilon_0(\theta)$ decreasing as power laws of the angle with respect to the jet orientation with indices a (energy) and b (Lorentz factor).
We assume that the emission site is located at the forward shock produced by the deceleration of the jet in an external medium with constant particle density n_{ext}. We neglect a potential contribution of the reverse shock at early times. We also do not include lateral spreading of the structure, which can impact the results when material becomes non-relativistic, and compute the dynamics at every latitude θ independently of the others.

• **Microphysics.** We assume that emission occurs at the forward shock and use the following parametrization: a fraction ϵ_e of the energy dissipated at the shock contributes to electron acceleration; and a fraction ϵ_B of that energy is injected in the amplified magnetic field. Electrons are initially injected with a distribution of Lorentz factors of slope $-p$. All electrons are accelerated in the process.

• **Radiative processes.** We model the synchrotron and SSC emission of the radiating electrons following the method described in Nakar, Ando & Sari 2009. This semi-analytic method allows to self-consistently compute the synchrotron power radiated by the electron population at the shock and the SSC power induced by the scatterings of the synchrotron photons on the seed electron population, while accounting for the Klein-Nishina regime. When Klein-Nishina effects are taken into accounts, the Inverse Compton (IC) scatterings also impact the shape of the distribution of the electron population's Lorentz factors; which in turn modifies the synchrotron spectrum shape. This method treats all possible situations in the slow and fast cooling regimes.
We extend this model by accounting for the maximum Lorentz factor at which electrons can be accelerated, γ_{max}. Indeed, to reach a Lorentz factor γ, the acceleration timescale $t_{acc}(\gamma)$ must be shorter than the timescale of radiative losses $t_{rad}(\gamma)$ and the dynamical timescale t_{dyn}, *e.g.* $t_{acc}(\gamma_{max}) = \min(t_{rad}(\gamma_{max});\ t_{dyn})$. This adds a high-energy cutoff in the synchrotron spectrum, subsequently leading to a cutoff in the SSC spectral shape.

• **Observing conditions.** We integrate the emitted power over the equal-arrival-time surfaces for an observer looking at the ejecta from a distance d_L, at a redshift z and with a viewing angle θ_{obs}.

3. Results

We show in this section the resulting light-curve and spectrum at the peak of the afterglow of GW170817. We use typical parameters inferred by other synchrotron light-curve fittings in the literature (see *e.g.* Duque et al. 2019), namely $\theta_c = 4°$; $E_{0,iso}(\theta < \theta_c) = 2 \cdot 10^{52}$ erg; $\Gamma_0(\theta < \theta_c) = 100$; $a = 4.5$; $b = 2.5$; $n_{ext} = 3 \cdot 10^{-3}$ cm^{-3}; $\epsilon_e = 10^{-1}$; $\epsilon_B = 10^{-4}$; $p = 2.2$; $\theta_{obs} = 22°$; $d_L = 42$ Mpc.

The light curve (left panel, Fig. 1, in blue) at 1 TeV only originates from SSC photons, as the maximum frequency for synchrotron photons $\nu_{max} = \nu_{syn}(\gamma_{max})$ has typical values

https://doi.org/10.1017/S1743921322000576 Published online by Cambridge University Press

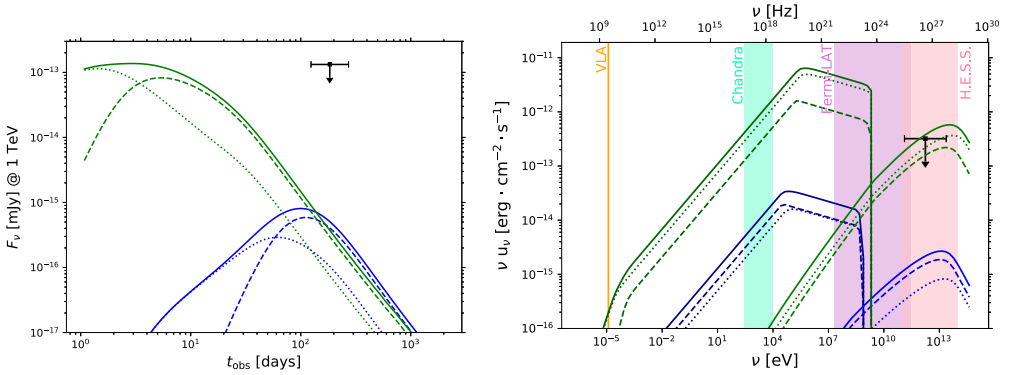

Figure 1. Light curves at $\nu_{\rm obs} = 1$ TeV (left) and spectra at peak (right) of GW170817's afterglow. Continuous line: total flux; Dashed line: contribution of the core; Dotted line: contribution of the sheath. In blue, $\theta_{\rm obs} = 22°$ ($t_{\rm peak} = 99$ days, reference value); In green, $\theta_{\rm obs} = 9°$ ($t_{\rm peak} = 2$ days, see the discussion). Refer to the text for details on the other parameters used. H.E.S.S. flux upper limit between 124 and 272 days is indicated in black and taken from HESS collaboration 2020. Shaded regions correspond to the energy ranges of the VLA, Chandra, Fermi-LAT and H.E.S.S., from lower to higher energies.

at ~ 1 GeV (right panel, Fig. 1, in blue). The effects of the lateral structure and the off-axis viewing angle can be seen at early times where the flux density is dominated by the emission from the lateral structure (sheath). Peak emission at 1 TeV is attained at $t_{\rm peak,SSC} = 99$ days, slightly earlier than in radio and X-rays ($t_{\rm peak,syn} = 112$ days), owing to the evolving efficiency of IC scatterings. Further analysis with data fitting will provide better parameter inference and thus peak time. At the peak time, the magnetic field in the core of the jet is predicted to be $\mathrm{B}'_{\rm core} \sim 360\mu$G (comoving frame), which is compatible with the lower limit from the HESS collaboration 2020 ($\sim 24\mu$G).

As can be seen on the spectrum (right panel, Fig. 1, in blue), access to the SSC component of the afterglow requires observations in the GeV-to-TeV domain, currently probed by *Fermi*-LAT, H.E.S.S. and MAGIC. However, the very weak flux intensity is not yet detectable by current instruments for a GW170817-like event.

4. Discussion

As highlighted by the simulated light curve of GW170817's afterglow, the flux at 1 TeV is two orders of magnitude below the upper limit put by the H.E.S.S. observation. This is due to two limiting factors: (i) a large viewing angle $\theta_{\rm obs}$; (ii) an intrinsic weak SSC component, as electrons at $\gamma_{\rm c}$, responsible for the peak of the synchrotron emission in X-rays, are already deeply in the Klein-Nishina regime, *i.e.* $\gamma_{\rm c} h\nu_{\rm c}/m_{\rm e}c^2 \gg 1$. In the following discussion, we therefore address the flux predictions for an event with similar parameters except for two more favourable conditions: a less off-axis observation or a denser environment. The second case allows to escape a too deep Klein-Nishina regime, which scales as $\gamma_{\rm c} h\nu_{\rm c}/m_{\rm e}c^2 \propto (\epsilon_{\rm B}\ n_{\rm ext})^{-5/2}$ in a uniform medium. Both situations lead to brighter afterglows peaking at earlier times, in the first case because the time needed to probe the central regions of the jet when it is seen more on-axis is shorter; and in the second case because the deceleration of the jet is more efficient as the medium density increases. A major difference is that increasing $n_{\rm ext}$ increases the intrinsic ratio $u_{\rm SSC}/u_{\rm syn}$, whereas the geometrical effect of the viewing angle is similar for both components of the spectrum. In the case of GW170817, a detection at peak time would have been possible with H.E.S.S. for viewing angles below $\sim 9°$ (see green curves, Fig. 1) or for densities $n_{\rm ext} \geq 1$ cm^{-3}. GW170817-like events occurring in environments with

https://doi.org/10.1017/S1743921322000576 Published online by Cambridge University Press

$n_{\rm ext} = 1$ cm^{-3} (resp. 100 cm^{-3}) would be detectable up to 110 Mpc (resp. 260 Mpc) with the CTA.

The consequences are twofold. First, a higher $n_{\rm ext}$ favours higher flux afterglows, especially in the SSC energy range, which leads to easier detections. Second, the different behaviour of the SSC component of the spectrum relative to $\theta_{\rm obs}$ and $n_{\rm ext}$ provides a way to break model degeneracies between these parameters. High-energy observations of afterglows will thus be of prime interest to uncover the details of their physical nature.

Interestingly, some arguments (summarized in Duque et al. 2020) hint towards an existing population with short merger time which remain close to their formation site, with a likely higher density. From a theoretical perspective, efficient common envelope phases (*e.g.* Dominik et al. 2012) or favorable supernovae kicks (*e.g.* Kalogera 1996) could lead to short merger times. Observations of galactic systems with merger times below 100 Myrs, the high abundance of r-process elements in some old stars, or some GRB afterglows that are best fitted by high density environments are many indicators that this population may exist. If it does, the afterglow peak luminosities are brighter and should therefore be over-represented in the sample of observations (Duque et al. 2020).

5. Conclusions

Our results show that GW170817's afterglow in the TeV domain was probably very weak. They comply with the upper limit of the H.E.S.S. observation at the radio peak time. Our numerical integration method uses a jet with a lateral structure and extends the emission spectrum to high energies *via* the SSC process, taking into account the Klein-Nishina regime and the maximum Lorentz factor of accelerated electrons. Our study shows that an increasing external density leads to an increase in the ratio $u_{\rm SSC}/u_{\rm syn}$, allowing to break degeneracies with viewing angle effects if observations in both spectral regimes are available. Finally, high-energy observations will be a prime tracer of fast-merging systems in higher density environments.

References

Abbott, B. P., Abbott, R., Abbott, T. D., et al. 2017a, *PhRvL*, 119, 161101
Abbott, B. P., Abbott, R., Abbott, T. D., et al. 2017b, *ApJL*, 848, L12
Cherenkov Telescope Array Consortium 2019, *Science with the Cherenkov Telescope Array.*, Published by World Scientific Publishing Co. Pte. Ltd., ISBN no.9789813270091
Dominik, M., Belczynski, K., Fryer, C., et al. 2012 *ApJ,* 759, 52
Duque, R., Daigne, F. & Mochkovitch, R. 2019, *A& A,* 631, A39
Duque, R., Beniamini, P., Daigne, F., et al. 2020, *A& A,* 639, A15
Ghirlanda, G., Salafia, O. S., Paragi, Z., et al. 2019, *Science*, 363, 6430, 968–971
Gill, R. & Granot, J. 2018, *MNRAS*, 478, 4128-4141
Goldstein, A., Veres, P., Burns, E., et al. 2017, *ApJL*, 848, L14
Hajela, A., Margutti, R., Alexander, K. D., et al. 2019, *ApJL*, 886, L17
H. E. S. S. Collaboration 2020, *ApJL*, 894, L16
Kalogera, V. 1996, *ApJ*, 471, 352
Mooley, K. P., Deller, A. T., Gottlieb, O., et al. 2018, *Nature*, 561, 7723, 355–359
Nakar, E., Ando, S. & Sari, R. 2009, *ApJ*, 703, 675-691
Savchenko, V., Ferrigno, C., Kuulkers, E., et al. 2017, *ApJL*, 848, L15
Tanvir, N. R., Levan, A. J., González-Fernández, C., et al. 2017, *ApJL*, 848, L27
Troja, E., van Eerten, H., Zhang, B., et al. 2020, *MNRAS*, 498, 5643-5651
Villar, V. A., Guillochon, J., Berger, E., et al. 2017, *ApJL*, 851, L21

https://doi.org/10.1017/S1743921322000576 Published online by Cambridge University Press